ELSEVIER

Journal of Crystal Growth 182 (1997) 281–291

JOURNAL OF CRYSTAL GROWTH

Influence of the surface morphology on the relaxation of low-strained $In_xGa_{1-x}As$ linear buffer structures

J.F. Valtueña[a,*], A. Sacedón[a], A.L. Alvarez[a], I. Izpura[a], F. Calle[a], E. Calleja[a], G. MacPherson[b], P.J. Goodhew[b], F.J. Pacheco[c], R. García[c], S.I. Molina[c]

[a] *Department Ingeniería Electrónica, ETSI Telecomunicación, UPM, Ciudad Universitaria s/n, 28040 Madrid, Spain*
[b] *Department of Materials Science and Engineering, University of Liverpool, Liverpool L69 3BX, UK*
[c] *Department Ciencia de Materiales e IM y QI Universidad de Cádiz, Puerto Real, 11510 Cádiz, Spain*

Received 15 January 1997; accepted 22 May 1997

Abstract

The relaxation of low-strained InGaAs linear-graded buffer layers up to 30 and 60% In content grown on GaAs substrates is studied. Strain-limited designs allow to preserve bidimensional (2D) growth mode with a relaxation driven by dislocation multiplication for large thickness, as in the case of single layers. However, it is shown that low-strained linear buffer layers are not able to inhibit tridimensional (3D) growth mode. Under standard growth conditions (500°C), the surface morphology evolves from a near-flat one for samples up to $x = 0.3$, to a rough one at higher In content, characterised by saw-tooth morphology with well-defined facets. The development of the surface roughness changes the strain relaxation mechanism from dislocation multiplication inside the layer to surface elastic strain relaxation plus surface nucleation and a high density of threading dislocations. A constant surface strain in linear grades during all the dislocation-driven relaxation is proposed to allow the observed 2D to 3D transition. The influence of the grading rate, composition steps, and growth temperature on the surface morphology and the relaxation are analysed. Appropriate growth conditions and buffer design up to high Indium content allow to produce structures with improved structural and optical quality.

Keywords: InGaAs; Buffer layers; Low strain; Relaxation mechanisms; Growth mode

1. Introduction

$In_xGa_{1-x}As$ graded buffer layers with an adjustable lattice parameter have a great interest for the integration of optically active devices operating at different wavelengths on commercial GaAs substrates. The design of optimum metamorphic structures involves the control of strain relaxation processes as well as surface morphology.

In the last few years many efforts have been made in the study of the interaction between the surface

* Corresponding author. Fax: +34 1 3367323; e-mail: valtu@die.upm.es.

PII S0022-0248(97)00377-1

morphology of strained layers, the growth mode, and the mechanisms of strain relaxation [1–10]. These works were focused mainly on the layers of constant composition for different mismatch with the substrate; it was found, however, that for high mismatches single layers do not behave in a predictable way. Complex structures like composition-graded or step-graded buffers are needed to control the lattice parameter at the surface without degrading the quality for further growth of active layers and devices [3, 11]. It is therefore important to extend the studies of the relaxation and growth mode evolution to those complex buffer structures. In this paper, we study the relaxation mechanisms acting on InGaAs linear-graded buffer structures grown on GaAs substrates.

The relaxation mechanism in strained systems consists of a competition between two main processes: dislocation multiplication (by spiral or Frank–Read sources) and surface roughening (grooves or islands). Although both processes could work simultaneously, in most of the cases only one of them drives the relaxation and the growth mode. This has been explained by Tersoff and LeGoues [6, 7] in terms of a strain (ε) dependence of the barrier energy (ΔG) for both processes, being proportional to ε^{-1} and ε^{-4} for multiplication and island development, respectively. For single layers, they show that when dislocation multiplication operates before roughening (low-strained layers) it is able to completely stop the island nucleation by decreasing the strain of the layer, and they predict that linear buffer layers should behave in the same way.

The transition from 2D to 3D growth mode appears in $In_xGa_{1-x}As$ single layers grown at 500°C on GaAs(0 0 1) for $x > 0.25$ (equivalent to a strain of 0.018) [12]. It is noticeable that the transition of the surface morphology depends on the growth conditions [8, 13, 14]. This constraint will also affect the linear-graded structures (grades), limiting design parameters like the initial In composition or the grading rate for certain growth conditions. Flat surfaces are expected to be obtained if the surface strain in grades does not surpass the critical value for 3D growth in single layers under standard growth conditions. In this case, a controllable strain relaxation should take place and the lattice parameter could be predicted [11].

Relaxation by dislocation multiplication on gradual buffer layers operates when the product of the average strain in the graded layer and its thickness ($\varepsilon \times t$) reaches the value of the relaxation constant ($K = 0.8$ nm) [15–17], at which point misfit dislocations appear at the strained–unstrained interface. The relaxation proceeds maintaining a strained (dislocation-free) region on the top of the structure. This layer accumulates the strain energy to keep the multiplication process operating and a constant strain value is maintained just at the surface [18, 19]. The XTEM images, especially of this top region, and the surface AFM images will allow us to directly determine any change in the relaxation mechanism.

This paper focuses on the influence of the design parameters and the growth temperature on the surface morphology, as well as the relaxation mechanisms in low-strained linear grades. We have designed a series of linear buffer structures with different strain levels under $\varepsilon = 0.018$ (by changing the In profile as a function of the grading rate and the introduction of composition steps) for two final In compositions. The expected relaxation of this graded buffer driven by the relaxation process should allow to obtain high In content layers keeping a low surface strain, since the large strain required in single layers of the same composition is avoided. However, we have found evidence of a growth mode evolution from layer by layer to a particular layer + islands when the In content is increased up to 60%. This change in the growth mode determines the relaxation mechanism, the modification of the dislocation distribution and the crystal quality of the structures. Low-temperature growth allows us to control the surface roughness and to verify the dislocation multiplication models for samples up to $x = 0.6$ In content.

The paper is organised as follows: the sample details and experimental techniques are summarised in Section 2. The experimental results for samples up to $x = 0.3$ and $x = 0.6$ are described in Section 3, and discussed in Section 4. Section 5 is devoted to an optimised low-temperature structure. The main conclusions of this work are summarised in Section 6.

2. Experimental procedure

Six InGaAs structures were grown on (0 0 1) on-axis GaAs substrates, by molecular beam epitaxy (MBE) using solid sources and tetrameric As_4, with a V/III flux ratio of 3, and a constant GaAs growth rate of 0.7 μm/h (i.e. giving an increasing growth rate for higher In content). In all the samples the GaAs substrate was desoxidated at 600°C and a GaAs buffer layer of 300 nm was grown at 500°C to obtain a clean and flat surface before the InGaAs graded-layer deposition. The growth temperature of the InGaAs buffer layer was 500°C except for sample *F* 450°C.

The sample structure is described in Table 1, samples A and B were grown up to $x = 0.3$ with two different gradients of the In composition: $g_{rate} = 30\%$ In μm^{-1} and $g_{rate} = 60\%$ In μm^{-1}. Four samples (C, D, E and F) were grown up to $x = 0.6$. Samples C and D are linear grades with the same gradient as samples A and B, respectively. In samples E and F, both with the same structure, a composition step (from 30% In to 35% In) was introduced in a grading of $g_{rate} = 60\%$ In μm^{-1}, and the growth temperature was changed from 500°C (sample E) to 450°C (sample F). The predicted maximum strain in the layer is 0.0065 and 0.008 for the grading rates (g_{rate}) 30% In μm^{-1} and 60% In μm^{-1}, respectively, and 0.011 for the step-graded samples (E and F).

The surface morphology was analysed by atomic force microscopy (AFM) in air at room temperature with a "Digital Instrument Nanoscope III" in contact mode, scanning at 4 Hz with a constant force of 0.06 Nm^{-1}. The defect characterisation was performed by cross-sectional and plan-view transmission electron microscopy (XTEM and PVTEM, respectively) with a JEOL 1200-EX operating at 120 KV. The XTEM specimens were mechanically thinned (by grinding, dimpling and polishing), and subsequently, subjected to an Ar^+ ion milling. The PVTEM specimens were prepared by chemical etching after the mechanical thinning. The optical quality was studied by photoluminescence spectroscopy (PL), with the samples cooled down to 14 K in a closed cycle helium cryostat. The 488 nm line of an Ar^+ laser was used for excitation, and the emission was analysed by a Jovin–Yvon 25 cm monochromator and detected by a liquid N_2-cooled Ge photodetector using synchronous lock-in techniques.

3. Results

First, we will study the structural behaviour of the samples grown at 500°C, separately for samples with $x = 0.3$ and 0.6 final In composition. The PL measurements will be presented afterwards for the sake of clarity.

3.1. Samples up to $x = 0.3$

XTEM images of samples A ($g_{rate} = 30\%$ In μm^{-1}) and B ($g_{rate} = 60\%$ In μm^{-1}) show a densely packaged dislocation region at the bottom

Table 1
Summary of sample structure. AFM mean roughness results, PL amplitude, and TD correlation

Sample	Final In composition	Internal step	Grading g_{rate} (% In μm^{-1})	Substrate temperature (°C)	Wavelength grooves (nm)	Height grooves (nm)	Threading dislocations (cm^{-2})	PL intensity (a.u.)
A	0.3	–	30%	500	50–500[a]	8	$< 10^6$	1
B	0.3	–	60%	500	600	10	$< 10^6$	0.25
C	0.6	–	30%	500	1000	80	$\sim 10^8$ [b]	1×10^{-4}
D	0.6	–	60%	500	650	100	$\sim 10^8$ [b]	5×10^{-5}
E	0.6	0.30–0.35	60%	500	400	40	$\sim 10^8$ [b]	0.001
F	0.6	0.30–0.35	60%	450	450	5	$< 10^6$	0.09

[a]For sample A grooves wavelength is not well defined.
[b]Threading dislocations only appear under the surface troughs.

of the graded structure, followed by a well-defined dislocation-free top region, as shown for sample A in Fig. 1a. PVTEM reveals that the misfit dislocations in the relaxed region are isotropically distributed. The dislocation network is mainly constituted ($\sim$80%) by 60° misfit dislocations (with Burgers vectors $a/2\langle 0\,1\,1\rangle$) the remaining $\sim$20% being edge dislocations ($a/2\langle 1\,1\,0\rangle$), probably originated as a result of the reactions between 60° dislocations [11, 19]. The threading dislocation density is below the detection limit of the system ($<10^6$ cm^{-2}).

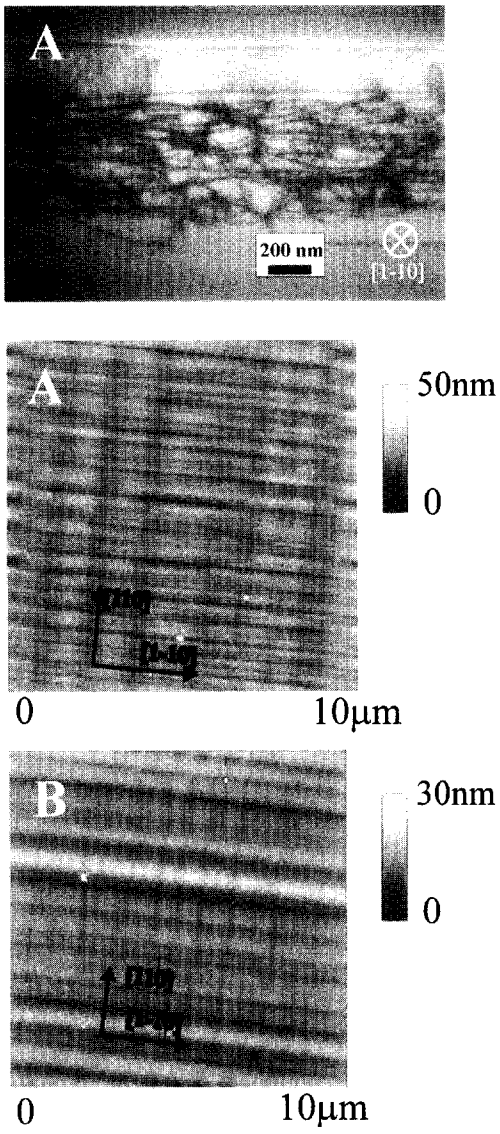

Fig. 1. (a) Cross-sectional [1 − 1 0] TEM (bright field) of sample A showing a distributed dislocation arrangement and the dislocation free top region. AFM images of samples up to 30% In content with different grading rates. (b) 30% In μm^{-1} (sample A), (c) 60% In μm^{-1} (sample B). Striations appear elongated in the [1 − 1 0] direction.

The predictions for the thickness of the dislocation-free regions are 298 and 195 nm, and the observed values are 300 and 150 nm for samples A and B, respectively. The small deviations are related to an incomplete relaxation of the bottom region due to dislocation interactions. The observed dislocation arrangement and strain distribution are in good agreement with theoretical models and experimental results of a relaxation driven by dislocation multiplication in a layer-by-layer growth mode [11, 18, 19].

The AFM images for samples A and B (Fig. 1b and Fig. 1c) show a smooth surface roughness formed by striations extended along the $\langle 1\,1\,0\rangle$ directions (cross-hatched pattern). The striations show a preferential orientation: when aligned along [1 − 1 0] direction, they are deeper and better defined, with a mean height of 8 and 10 nm for samples A and B, respectively [20]. For sample B where the striations are homogeneously distributed, a mean striation wavelength of 600 ± 50 nm is estimated. The striations can be considered, as discussed below, as the initial stages of the transition to 3D growth mode.

3.2. *Samples up to x = 0.6*

When the final In content of the described structures is increased up to $x = 0.6$, the structural and optical properties of the gradual buffer layers change radically.

AFM images for samples C ($g_{\text{rate}} = 30\%$ In μm^{-1}) and D ($g_{\text{rate}} = 60\%$ In μm^{-1}) are shown in Fig. 2. A sharp development of the surface roughness as compared to samples up to $x = 0.3$ is observed. The surface is formed by deep grooves perfectly aligned along the [1 − 1 0] direction, some of them are visible across the whole sample. In contrast, very slight features are aligned in the [1 1 0] direction, appearing as an amplitude modulation of those along the [1 − 1 0]. The grooves

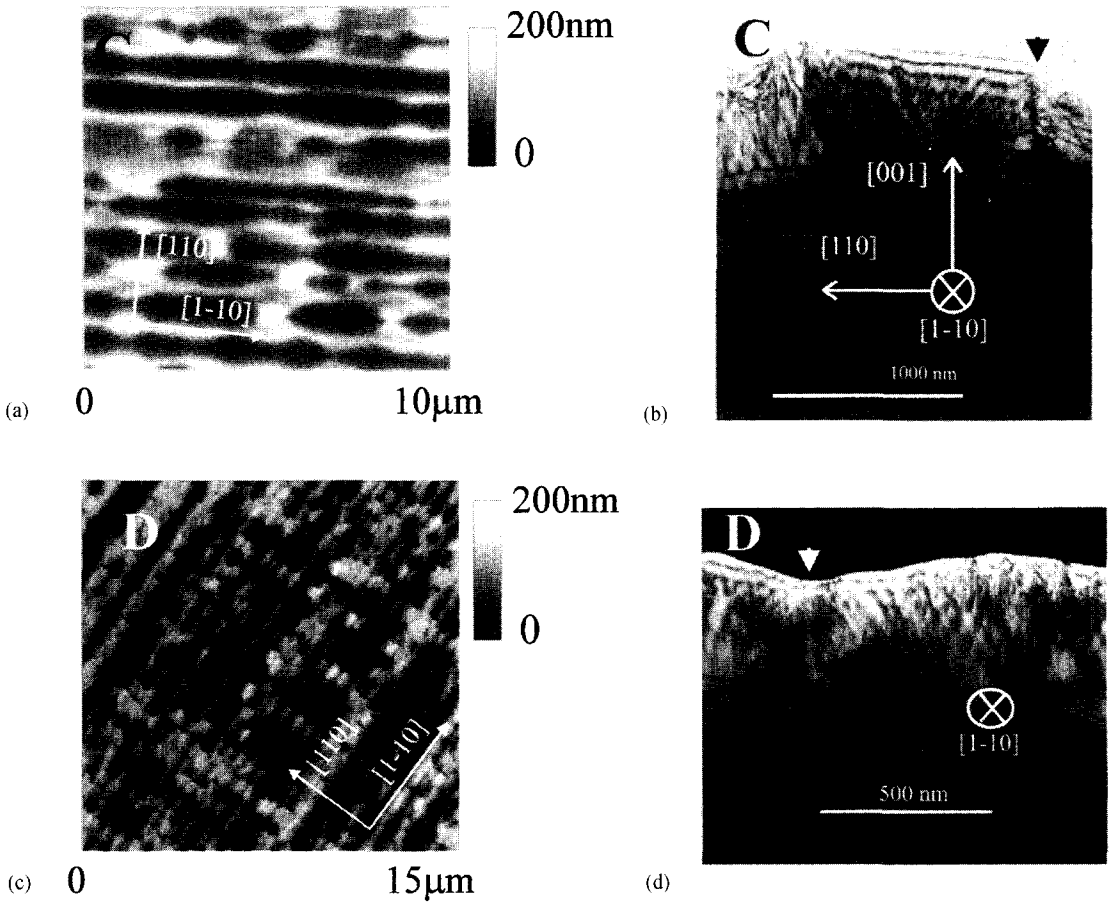

Fig. 2. AFM and cross-sectional [1 − 1 0] TEM images for grades up to 60% In content. (a) and (b) AFM for a grading of 30% In μm^{-1} (sample C). (c) and (d) for a grading of 60% In μm^{-1} (sample D). Clear striations along the [1 − 1 0] direction and their correlation with the dislocation arrangement showing pile-ups and dislocation interactions under the surface valleys are shown.

show a periodic pattern, with a mean striation height of 80 ± 10 and 100 ± 10 nm, and a wavelength of 1000 ± 50 and 650 ± 50 nm, for samples C and D, respectively.

The XTEM images of samples C and D, taken orthogonal to the grooves ([1 − 1 0] projection), are also shown in Fig. 2. In addition to the surface grooves a change in the dislocation arrangement is observed, and the dislocation-free character of the top region disappears. Dislocation pile-ups appear close to the surface and they are spatially correlated with the valleys of the deepest grooves, as shown in the images by arrows pointing to dark vertical bands. These dislocation pile-ups are densely packaged along the [0 0 1] direction, forming a "grain boundary". The nature of these dislocations is different from the one previously observed: they are 90° misfit dislocations with $a/2\langle 1\,1\,0\rangle$ Burgers vectors. A very strong interaction with those 60° misfit dislocations lying along the [1 1 0] direction is observed. The pile-up acts as a barrier for orthogonal gliding dislocations as can be inferred from Fig. 2b and Fig. 2d, in which threading dislocations are seen near the grain boundary. The nature of the Burgers vector and their arrangement in pile-ups located at the bottom of the grooves suggest that these dislocations are nucleated at the surface, they are no longer isotropically distributed

along the [1 1 0] and [1 − 1 0] directions, and show the same anisotropy observed in the rippled surface. The XTEM images reveal a faceted surface with a constant faceting angle of 16 ± 0.5°on each side of the groove, similar to the islands observed in highly strained growth [13, 21].

The previously observed increment of roughness with thickness, common to all buffer structures and growth techniques, suggests that the layer should be as thin as possible in order to reduce the amplitude of surface striations [11, 14]. The use of composition steps which increase the strain in limited regions allows to minimise the total thickness without high grading rates. A step of 5% In content was introduced in sample E between $x = 0.3$ and $x = 0.35$, and the grading was continued to the final composition of $x = 0.6$. The composition step was adjusted to keep surface strain under the 3D limit; when it is introduced, the strain sharply increases in the surface from 0.008 to 0.011. The step position in the buffer was chosen before the surface starts to develop deep striations (sample B). However, AFM and TEM images (Fig. 3) reveal a behaviour similar to that observed in samples C and D. The only relevant difference is the reduction of the groove amplitude (40 nm) and wavelength (400 ± 50 nm).

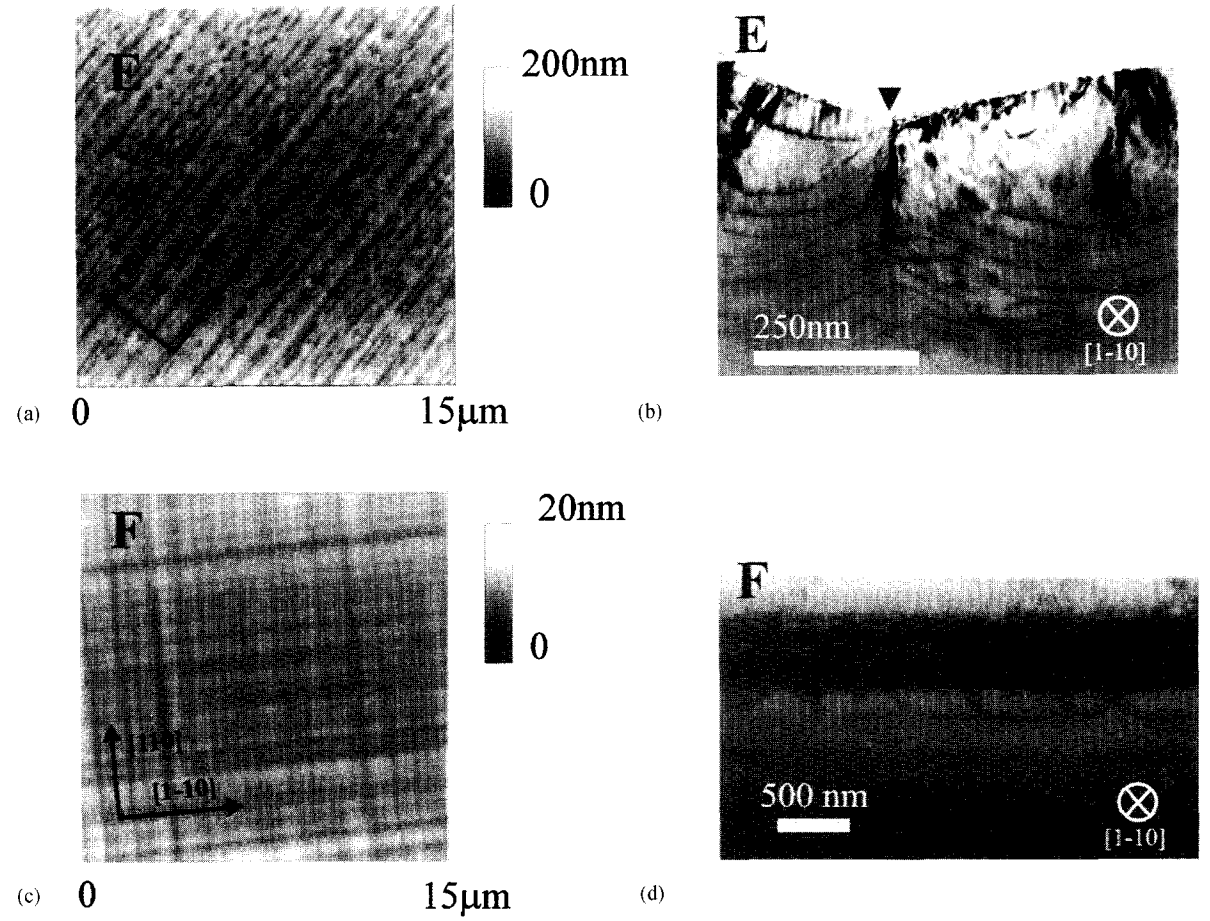

Fig. 3. AFM and cross-sectional [1 − 1 0] TEM images for samples E and F with the same structure (internal composition step, 60% In μm^{-1}, up to 60% In) grown at 500 and 450°C, respectively. For sample F, the surface is smoother and the interactions between dislocations and striations are not observed, giving rise to a dislocation-free top region.

3.3. PL assessment

The dislocation density in the top region plays a major role in order to determine whether the buffer layer is suitable for subsequent device fabrication. However, the threading dislocation density obtained by TEM is limited by their resolution. The behaviour of dislocations as nonradiative recombination centres and their strong influence on the PL spectra is well known [22, 23]. In all the samples, the PL signal is expected to arise from the dislocation-free top region, where the density of nonradiative recombination centres is lower, and the emission at higher energies from the bottom region (lower indium content) is absorbed. That is why the PL intensity has been used as an independent indicator in order to assess the quality of the dislocation-free top layer.

The low-temperature PL spectra of the different buffer layers is shown in Fig. 4, and intensity is summarised in Table 1. For samples grown at 500°C up to $x = 0.6$, the PL intensity is negligible (3–4 orders of magnitude lower) as compared to that obtained for samples up to $x = 0.3$. This result is not surprising due to the presence of higher density of threading dislocation segments in samples C, D and E. It indicates that the path for nonradiative recombination is directly related to threading dislocations or to grain boundaries

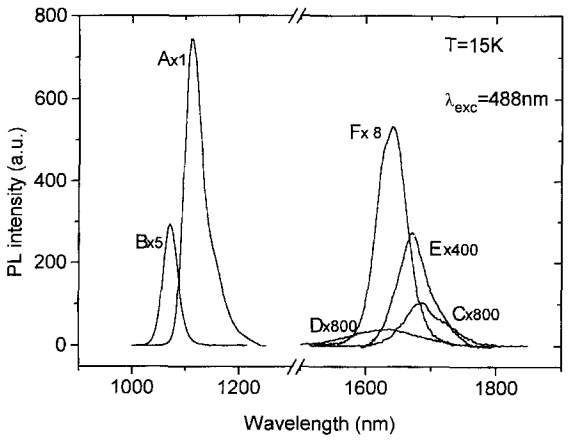

Fig. 4. Photoluminescence spectra of the different samples: A, B, E and F.

located in the top layer, and not to misfit dislocations parallel to the interface (relaxed region). This observation supports previous cathodoluminescence studies which show that dark defects are correlated with high-density dislocation packages [10, 24]. However, the improved intensity of sample E as compared with samples C and D (1 order of magnitude) is not yet understood.

4. Discussion

All the observed results show that the growth mode has changed from 2D (grades up to $x = 0.3$) to 3D for samples up to $x = 0.6$ which have been grown under the specified designs and conditions. Then it is possible to differentiate between two stages: in the first stage (2D growth mode) the multiplication of dislocations drives the relaxation process, and roughening is shown in their starting level. The second stage (3D growth mode) is characterised by the development of striations, the presence of threading dislocations and the faceted surface morphology, despite the low strain level which has been maintained during the growth.

In order to understand the relaxation process and its consequences in the structural and optical properties of the grades, the interaction between the different relaxation mechanisms has to be considered. For single layers (constant composition) both roughening and dislocation nucleation act as competitive relaxation processes: each one inhibits the occurrence of the other by increasing its activation barriers [6]. For moderate x, the dominant relaxation process is driven by the generation of misfit dislocations.

The main difference between linear grades and single layers is that, in the former, the surface strain is not reduced during relaxation, but keeps a constant value (as previously shown for the samples up to $x = 0.3$ [11, 19]). Thus, the competition between both relaxation mechanisms (dislocation and roughening) is removed: when dislocation nucleation drives the relaxation in the first stage, the roughening is not inhibited, and operates independently on the surface. Nevertheless, the low surface strain decreases the roughness growth rate (high activation energy $\Delta G \propto \varepsilon^{-4}$). Then roughening

evolves very slowly when compared with the sharp transition observed at island formation during S–K growth mode: samples up to $x = 0.3$ show the initial stages of roughness formation, even when they have been grown up to 1 μm (sample A). The low amplitude-to-wavelength ratio of the observed strained morphology ($A/\lambda < 0.02$) allows to neglect any relaxation contribution in samples A and B due to the surface roughness [25–27]. This fact could explain why the results closely follow the theoretical models for relaxation by dislocation multiplication.

However, in the second stage, the striations develop acting as an independent relaxation mechanism, the strain gradient on the surface increases and produces an enhanced surface diffusion. This contributes to a further increment of the striations amplitude, and justifies the observed dependence of striations amplitude on the sample thickness in a feedback process (from 8–10 nm for $x = 0.3$ to 80–100 nm for $x = 0.6$).

The influence of the buffer parameters on the striation morphology can be estimated by analysing the surface strain associated with the relaxation controlled by dislocations in the grades. As a first approximation, the relation of the surface strain (ε_s) with the grading rate (g_{rate}) will satisfy

$$\varepsilon_s = \beta\sqrt{2Kg_{rate}}, \tag{1}$$

where K is the relaxation constant, and the relation strain-%In is given by $\beta = 0.071\%\text{In}^{-1}$ [18, 19]. According to energy balance calculations, the critical wavelength (λ_c) for stable roughening [25, 27, 28] is given by

$$\lambda_c = \frac{\pi\gamma(1-\nu)}{2\mu(1+\nu)^2\varepsilon^2}, \tag{2}$$

where γ, μ, and ν are the surface energy, the shear modulus and the Poisson's ratio, respectively. From Eqs. (1) and (2) it follows that

$$\lambda_c = \frac{\pi\gamma(1-\nu)}{4\mu(1+\nu)^2\beta^2 Kg_{rate}}. \tag{3}$$

The constant strain at the surface produced by the dislocation-driven relaxation establishes a constant critical striation wavelength during the roughness development. It is important to notice the evolution of striations during growth: For sample B striations are well defined and their wavelength (600 nm) is kept constant during growth, almost equal to sample D up to $x = 0.6$ (650 nm). Eq. (3) shows an inverse relation between striation wavelength and the grading rate, which is qualitatively verified in samples C, D and E with a mean groove wavelength of 1000, 650, and 400 nm, respectively [29].

The amplitude of the striations for samples up to $x = 0.6$ is scaled with the groove wavelength (except for sample D due to island formation on the top of the grooves). This relation can be explained by the observed faceted morphology which limits the striation amplitude development [6, 30]. XTEM images show a triangular-like shape, with a contact angle of 16°. The striations induced at the surface present a faceted morphology similar to that shown by the islands generated in highly strained growth [13]. The size of the striations in our samples is scaled up compared with the islands, consistent with the lower strain of our samples.

The S–K growth mode produces results similar to those observed in our grades, but with some discrepancies. The surface morphology is defined by striations oriented along the [1 − 1 0] direction, as opposed to islanding or random oriented ripples. The asymmetric island morphology, reported by several authors [13, 21], has been shown to be the energetically stable solution for size perturbations of the optimum square island shape [30]. The preferential growth along the [1 − 1 0] direction could be due to the anisotropy of the energy for step-edge attachment between [1 1 0] and [1 − 1 0] kinks in the As-rich reconstruction on GaAs. However, it is not feasible to produce the long-order (several mm) alignment of striations observed in the first stages of growth (Fig. 1a and Fig. 1b). On the other hand, dislocations nucleate before roughening and could well be considered as the source of the surface morphology [31, 32]. The spatial link between surface grooves and misfit dislocations has not been observed for samples up to $x = 0.3$, probably due to the mobile character of the surface steps during growth and the generation of new dislocations.

In the second relaxation stage when striations have developed in amplitude ($A/\lambda \approx 0.1$), a clear correlation is observed between deepest grooves and dislocation pile-ups in the top-most region of the buffer layer. The rough morphology not only contributes to an elastic relaxation, but also the strain concentrates at the striation valleys introducing preferential nucleation sites for misfit dislocations [33]. The arrangement of the pile-ups along the [0 0 1] direction indicates a defined position of the troughs during surface evolution. This behaviour is equivalent to a direct 3D growth mode in high-strained systems: the islands reduce their inner strain and for low coverage no misfit dislocations are needed to relax the strain. At higher coverage, boundaries between islands provide a low-barrier path for dislocation nucleation where strain is accumulated [9, 21, 26, 34]. In both cases 90° dislocations are mainly observed. The dislocation configuration correlated with the surface striations indicates a process of surface nucleation. The presence of the observed dislocation arrangement constituted by $a/2\langle 1\,1\,0\rangle$ dislocations is not clear at present, because the mechanism associated with half-loops nucleation is unable to nucleate directly sessile $a/2\langle 0\,1\,1\rangle$ dislocations. A separate nucleation of Frank and Shockley partials has been proposed to produce complete 90° dislocations [35]. The pile-ups act as a barrier for the gliding of dislocations running normal to them. We suspect that this mechanism of interaction with the normal dislocation array is responsible for the high density of threading dislocations observed at the troughs ($\sim 10^8\ \mathrm{cm}^{-2}$) rather than threading segments coming from loops nucleation [5, 25, 36].

The aligned saw-tooth morphology, with a design modulated wavelength, suggests the potential application to obtain self-ordered pattern substrates with a geometry suitable for the fabrication of quantum wires.

5. The effect of the growth temperature

The final goal of this work is to obtain a buffer structure suitable for device integration. In order to improve buffer quality up to $x = 0.6$, it is necessary to avoid the development of the surface roughness. For a given surface chemical gradient, the growth rate of roughness can be reduced by decreasing growth temperature, as shown by flattened morphologies reported by several authors [5, 9]. The main effect expected when growth temperature is decreased is a reduction of the diffusivity, which limits the motion of the adatoms to reach locations which are energetically favoured. This is equivalent to decreasing the surface diffusion length, which has been shown to depend exponentially on temperature [5, 8, 13].

The same design of sample E (with an internal step) has been used to grow sample F at a reduced substrate temperature of 450°C for the InGaAs buffer layer. The AFM image in Fig. 3c shows a cross-hatched surface for sample F with a mean roughness of only 5 nm. The deep striations observed in sample E ($T_s = 500$°C) are no longer present, and only shallow ones appear comparable in amplitude to those obtained for samples up to $x = 0.3$ In content. The striation wavelength 450 ± 50 nm, is similar to that observed in sample E (400 ± 50 nm). The XTEM image (Fig. 3d) shows that the dislocations appear homogeneously distributed along the buffer layer with a dislocation-free top region 170 ± 10 nm thick (threading dislocation below $10^6\ \mathrm{cm}^{-2}$). It was not possible to observe the pile-ups present in other samples. Most of the observed dislocations have a Burgers vector of the type $a/2\langle 0\,1\,1\rangle$ and run along both $\langle 1\,1\,0\rangle$ directions parallel to the surface. The observed dislocation distribution in sample F is in agreement with the theoretical relaxation models driven by dislocation multiplication [18, 19]. The small deviations of the dislocation-free thickness from the relaxation model [19], around 10%, supposes an equivalent shift of 0.1% from the predicted lattice parameter in the strained region. It should be noticed that growth temperature modifies the roughness development (slower roughness growth rate) but the stability criteria for the striations wavelength, strain dependent, remain unaffected. This explains why samples E and F have almost the same striations wavelength, in spite of the change in the growth temperature and final structural characteristics.

The PL intensity of sample F shows an improvement (100 times) compared with sample E, and it is

comparable to the intensity of the samples up to $x = 0.3$, in agreement with the high structural quality.

These results show that the main relaxation process is not related to the surface shape when surface roughness is kept at low amplitude. However, in the samples grown at 500°C, where the surface plays an important role in the strain relaxation, the dislocation arrangement is not produced by multiplication process, but imposed by the surface roughness.

6. Conclusions

It has been shown that the low surface strain during the growth of graded buffer layers is not able to prevent the evolution of the flat surface to a striated morphology. Striations are equivalent to island formation in S–K growth mode for high-strained systems. The evolution to a S–K growth mode is produced by the action of a constant surface strain during dislocation-driven relaxation. In the first stages, low amplitude roughness is unable to modify the dislocation generation process and the relaxation. However, the surface slowly evolves during growth, giving rise to striations which contribute to modify the dislocation pattern. The roughness is characterised by long-range faceted striations, oriented along the [1 − 1 0] direction with potential application in quantum wire technology. The striation wavelength, dependent on design parameters (In composition profile) and roughening, can be controlled at low growth temperature. The relaxation, when driven by the multiplication of dislocations without any influence from the surface, allows to obtain high-quality structures, according to the relaxation models. The improved quality obtained for low-temperature buffer layers should encourage further work on the integration and development of devices with high Indium contents on GaAs substrates.

Acknowledgements

The financial support of CICYT project TIC95-0116 is acknowledged.

References

[1] A.G. Cullis, D.J. Robbins, A.J. Pidduck, P.W. Smith, J. Crystal Growth 123 (1992) 333.
[2] C.W. Snyder, B.G. Orr, D. Kessler, L.M. Sander, Phys. Rev. Lett. 66 (1991) 3032.
[3] D.J. Dunstan, P. Kidd, R. Beanland, A. Sacedón, E. Calleja, L. González, Y. González, F.J. Pacheco, J. Mater. Sci. Technol. (1996), in press.
[4] G. Macpherson, P.J. Goodhew, R. Beanland, Phylos. Mag. A 72 (1995) 1531.
[5] N. Grandjean, J. Massies, J. Crystal Growth 134 (1993) 61.
[6] J. Tersoff, F.K. LeGoues, Phys. Rev. Lett. 72 (1994) 3570.
[7] F.K. Legoues, P.M. Mooney, J. Tersoff, Phys. Rev. Lett. 71 (1993) 396.
[8] E.T. Klaus, H. Poog, J. Crystal Growth 135 (1994) 97.
[9] S. Guha, K.C. Rajkumar, A. Madhukar, J. Crystal Growth 111 (1994) 434.
[10] E.A. Fitzgerald, G.P. Watson, R.E. Proano, D.G. Ast, P.D. Kirchner, G.D. Pettit, J.M. Woodall, J. Appl. Phys. 65 (1989) 2220.
[11] P. Kidd, D.J. Dunstan, H.G. Colson, M.A. Lourenço, A. Sacedón, F. González-Sanz, L. González, Y. Gonzalez, R. García, D. González, F.J. Pacheco, P. Goodhew, J. Crystal Growth 169 (1996) 649.
[12] V. Krishnamoorthy, P. Rivas, R.M. Park, Appl. Phys. Lett. 58 (1991) 2000.
[13] K. Tillmann, D. Gerthsen, P. Pfundstein, A. Föster, K. Urban, J. Appl. Phys. 78 (1995) 3824.
[14] J.W.P. Hsu, E.A. Fitzgerald, Y.H. Xie, P.J. Silverman, M.J. Cardillo, Appl. Phys. Lett. 61 (1992) 1293.
[15] D.J. Dunstan, P. Kidd, L. Howard, R.H. Dixon, Appl. Phys. Lett. 59 (1991) 3390.
[16] D.J. Dunstan, P. Kidd, P.F. Fewster, N.L. Andrew, R. Grey, J.P.R. David, L. González, Y. González, A. Sacedón, F. González-Sanz, Appl. Phys. Lett. 65 (1994) 839.
[17] A. Sacedón, R. Beanland, H. Colson, E. Calleja, Appl. Phys. Lett., 1996, submitted.
[18] J. Tersoff, Appl. Phys. Lett. 62 (1993) 693.
[19] A. Sacedón, F. González-Sanz, E. Calleja, E. Muñoz, S.I. Molina, F.J. Pacheco, D. Araujo, R. Garcia, M. Lourenço, Z. Yang, P. Kidd, D. Dunstan, Appl. Phys. Lett. 66 (1995) 3334.
[20] Substrate cleavage edges have been used for ⟨1 1 0⟩ direction discrimination.
[21] A.G. Cullis, A.J. Pidduck, M.T. Emeny, Phys. Rev. Lett. 12 (1995) 2368.
[22] T.G. Andersson, Z.G. Chen, V.D. Kulakovskii, A. Uddin, T. Vallin, Appl. Phys. Lett. 51 (1987) 752.
[23] M. Grundmann, U. Lienert, J. Christen, D. Bimberg, A. Ficher-Colbrie, J.N. Miller, J. Vac. Sci. Technol. B 8 (1990) 751.
[24] D.H. Rich, T. George, W.T. Pike, J. Maserjian, F.J. Grunthaner, A. Larsson, J. Appl. Phys. 72 (1992) 5834.
[25] H. Gao, J. Mech. Phys. Solids 42 (5) (1994) 773.
[26] W.H. Yang, D.J. Srolovitz, Phys. Rev. Lett. 71 (1993) 1593.
[27] J. Grilhe, Acta Metallogr. (1993) 909.

[28] D.J. Srolovitz, Acta Metallogr. 37 (2) (1989) 621.
[29] To estimate the critical wavelength of sample E, it is necessary to use EC 2, including the grading surface strain and the strain due to the composition step.
[30] J. Tersoff, R.M. Tromp, Phys. Rev. Lett. 70 (1993) 2782.
[31] K.L. Kavanagh, M.A. Capano, L.W. Hobbs, J.C. Barbour, P.M.J. Marée, W. Schaff, J.W. Mayer, D. Pettit, J.M. Woodallo, J.A. Stroscio, R.M. Feenstra, J. Appl. Phys. 64 (1988) 4843.
[32] A.L. Alvarez, F. Calle, A. Sacedón, E. Calleja, E. Muñoz, R. García, L. González, P. Kidd, R. Beanland, P. Goodhew, Solid State Electron. 40 (1996) 647.
[33] M. Alberech, S. Christiansen, J. Michler, W. Dorsch, H.P. Strunk, Appl. Phys. Lett. 67 (1995) 1232.
[34] D.E. Jesson, S.J. Pennycook, J.M. Baribeau, D.C. Houghton, Phys. Rev. Lett. 11 (1993) 1774.
[35] Y. Chen, X.W. Lin, Z. Lillental-Wber, J. Washburn, J.F. Klem, J.T. Tsao, Appl. Phys. Lett. 68 (1996) 111.
[36] P.M. Marée, J.C. Barbour, J.F. van der Veen, K.L. Kavanagh, C.W.T. Bulle-Lieuwma, M.P.A. Viegers, J. Appl. Phys. 62 (1987) 4413.